# Pseudopotentials for Orbital-Free DFT: Capturing Nonlocality and Correcting Functional Approximants

Valeria Rios-Vargas,<sup>1, a)</sup> Ezekiel Oyeniyi,<sup>2</sup> Xuecheng Shao,<sup>3</sup> Wala Fathelrahman Ibrahim Elsayed,<sup>4</sup> Sunday Joseph Ogenyi,<sup>4</sup> Alex Okello,<sup>5</sup> and Michele Pavanello<sup>1, 6, b)</sup>

- <sup>1)</sup>Department of Physics, Rutgers University, Newark, NJ 07102, USA
- <sup>2)</sup>Department of Physics, University of Ibadan, Ibadan, Nigeria
- <sup>3)</sup>Key Laboratory of Material Simulation Methods & Software of Ministry of Education, College of Physics, Jilin University, Changchun 130012, PR China
- <sup>4)</sup> Condensed Matter Section, East African Institute for Fundamental Research (EAIFR), University of Rwanda, Kigali, Rwanda.
- <sup>5)</sup>Department of Science and Vocational Education, Faculty of Education, Lira University, Lira, Uganda
- <sup>6)</sup>Department of Chemistry, Rutgers University, Newark, NJ 07102, USA

(Dated: 26 November 2025)

Developing reliable pseudopotentials for orbital-free density functional theory (OF-DFT), especially for transition metals, remains a significant challenge. In this study, we provide a theoretical framework for analyzing pseudization strategies for OF-DFT calculations. From the analysis arises a proposed pseudization method which involves constructing local pseudopotentials by targeting existing Kohn–Sham DFT pseudopotentials through an optimized effective potential procedure. We produce four distinct sets of local pseudopotentials and evaluate their accuracy and transferability on the transition metal elements. Our results indicate a substantial improvement over previously available pseudopotentials. Although current OF-DFT functionals still only reach a qualitative accuracy for transition metals, our newly developed pseudopotentials provide a rigorous framework for further methodological advancements.

 $<sup>^{\</sup>rm a)}$ Electronic mail: valeria.rios@rutgers.edu

b) Electronic mail: m.pavanello@rutgers.edu

#### I. INTRODUCTION AND BACKGROUND

Among all approaches to modeling materials at the atomic level, Density Functional Theory as formulated by Kohn and Sham<sup>1</sup> (KS-DFT) stands out for its impact. Its most widely used methods have so far been cited over 200,000 times<sup>2</sup>. KS-DFT's implementations offer a good compromise between accuracy and computational cost. However, independently from the choice of the underlying approximations, it becomes too computationally expensive when large, realistically-sized systems (e.g., quantum dots, proteins and complex materials interfaces) are targeted. The reason for this is the unavoidable costs of building and diagonalizing the KS Hamiltonian matrix. In particular, diagonalizations carry a cost of  $\mathcal{O}(N^3)$  number of operations, where N is measure of system size. There are many approaches that tackle KS-DFT's steep computational scaling<sup>3-6</sup>. Among them, a promising alternative is orbital-free DFT (OF-DFT)<sup>7,8</sup>.

OF-DFT is based on the same theoretical footing as KS-DFT<sup>1</sup>. In particular, it borrows KS-DFT's expression for the total electronic energy given as a functional of the electronic density:

$$E[n] = T_s[n] + E_{Hxc}[n] + \int v_{ext}(\mathbf{r})n(\mathbf{r})d\mathbf{r}$$
(1)

where  $T_s$ ,  $E_{Hxc}$ , and  $v_{ext}(\mathbf{r})$  are the noninteracting kinetic energy, the Hartree exchangecorrelation (xc) energy, and the interaction with the external potential (typically the Coulomb electron-nuclear attraction potential), respectively. The noninteracting kinetic energy is given in terms of KS orbitals (single particle functions, hence the "s" subscript) as follows

$$T_s[n] \equiv T_s[\{\phi_i[n]\}] = -\frac{1}{2} \sum_i n_i \langle \phi_i | \nabla^2 | \phi_i \rangle, \tag{2}$$

where  $n_i$  are occupation numbers. The electron density is simply

$$n(\mathbf{r}) = \sum_{i} n_i |\phi_i(\mathbf{r})|^2 \tag{3}$$

The Hartree functional is defined as the electronic Coulomb self-repulsion,  $E_H[n] = \frac{1}{2} \int \frac{n(\mathbf{r})n(\mathbf{r'})}{|\mathbf{r}-\mathbf{r'}|} d\mathbf{r} d\mathbf{r'}$  and the xc functional,  $E_{xc}[n]$  is the energy term that is added to  $T_s[n]$ ,  $E_H[n]$  and  $\int v_{ext}(\mathbf{r})n(\mathbf{r})d\mathbf{r}$  to recover the total electronic energy.

Following from Eq. (3), we can use the KS orbitals as variational functions to minimize

the total energy, leading to the canonical KS equations

$$-\frac{1}{2}\nabla^2\phi_i(\mathbf{r}) + v_s(\mathbf{r})\phi_i(\mathbf{r}) = \varepsilon_i\phi_i(\mathbf{r})$$
(4)

where  $v_s(\mathbf{r}) = v_{Hxc}[n](\mathbf{r}) + v_{ext}(\mathbf{r})$  defining the Hxc potential as a functional derivative,  $v_{Hxc}[n](\mathbf{r}) = \frac{\delta E_{Hxc}}{\delta n(\mathbf{r})}$ .

In OF-DFT, the noninteracting kinetic energy,  $T_s$ , is evaluated approximately by a pure density functional, which we call henceforth the kinetic energy density functional or KEDF. The accuracy of OF-DFT depends on the KEDF  $T_s[\rho]$ , with magnitude equal to the total energy, for highly inhomogeneous electron densities the devolopment of KEDFs is still a challenging task, however there are good functionals sunch as LMGP<sup>9,10</sup>, Huang-Carter (HC)<sup>11</sup>, and revHC<sup>12</sup> which provides one of the most accurate descriptions of metallic systems currently available. Using KEDFs allows the energy minimization of the functional in Eq. (1) to be based solely on the electron density, completely bypassing the KS orbitals, and generally leading to algorithms of linear scaling complexity.<sup>7</sup>.

One thorn on the side of OF-DFT has persisted. Namely the handling of the electronion interaction. While this seems a non-issue (the  $v_{ext}(\mathbf{r})$  is conceptually trivial), when approaching condensed phases the pseudopotential (PP) approximation is usually invoked<sup>13–19</sup>. Natural basis functions used to expand the KS orbitals for materials are plane waves,  $\chi_{\mathbf{k}}(\mathbf{r}) = \frac{1}{\sqrt{\Omega}}e^{i\mathbf{k}\cdot\mathbf{r}}$ , where  $\mathbf{k}$  denotes a wave vector in the reciprocal lattice, and  $\Omega$  is the real-space volume of the primitive cell such that the plane waves are orthonormal over  $\Omega$ . To maintain a reasonable number of plane waves, a cutoff is imposed  $|\mathbf{k}| < k_{max}$ . Thus, PPs achieve two objectives: (1) at the expense of introducing nonlocality in the pseudopotential, they remove the need to explicitly consider core electrons as these are, in most applications, chemically inert; and (2) they eliminate the singularity of the Coulomb electron-nuclear potential at the nuclear positions<sup>20,21</sup>.

Unfortunately, accurate and transferable nonlocal PPs (NLPPs) commonly used in KS-DFT, are not applicable to OF-DFT because they require KS orbitals to couple to the nonlocal part of the PP. In OF-DFT, as we have seen, orbitals are not immediately available.

Although we refer to recent reviews for additional details<sup>7,8</sup>, in the past decades several attempts have produced effective local PPs (LPPs, hereafter) that have opened OF-DFT's applicability to main group metal elements, groups III-V elements third row and below, and a selected number of transition metal elements (such as Ag)<sup>15,18,22–24</sup>.

The guiding principles to build LPPs have been to employ them in a KS-DFT calculation (i.e., with exact  $T_s$ ) imposing it to reproduce the electron density, lattice constant and even the band structure of solids 18,22,23. For those elements for which this is possible, it is said LPPs can be employed in OF-DFT calculations. It is certainly surprising that band structures can be reproduced in pseudopotential calculations having only a local part. However, in many cases it was shown to be possible<sup>25</sup>. It turns out that LPPs can be successfully constructed for the main-group elements mentioned above and also for a large array of transition metals (provided that the semicore states are excluded from the pseudization<sup>17</sup>). The most accurate LPPs available to date for transition metal elements are the recently developed highly accurate LPPs by the Huang group<sup>17</sup>. The valence density of transition metals consists of both localized d electrons and delocalized s-p conduction electrons, a regime in which most existing KEDFs are constructed from the response of homogeneous or nearly homogeneous electron gas struggle to provide accurate kinetic energies. In addition, reliable LPPs must account for semicore s-like states that lie close in energy to the valence d bands and influence bonding and screening. Since OF-DFT approximates  $T_s[\rho]$  strictly as a functional of the electron density, it lacks explicit angular-momentum dependence and therefore cannot distinguish d-state character from s or p contributions. These combined factors explain why transition metals are particularly demanding within OF-DFT and motivate the construction of pseudopotentials specifically designed to mitigate these limitations. In this work, semicore states are not explicitly included in the optimization procedure to preserve numerical stability across the periodic table; however the proposed methodology corrects the KEDF and the PP at the same time by reproducing correct scattering properties and remain transferable in bulk and cluster environments.

A flaw, however, is that the LPPs have so far been developed based on comparison between KS-DFT calculations with LPPs and KS-DFT calculations with NLPPs. When the band structure and other observables agree between the two, the LPP is deemed suitable for OF-DFT simulations. However, this procedure does not account for the differences between OF-DFT KEDFs and the exact  $T_s[n]$  from KS-DFT. In this work we aim at addressing this flaw.

In fact, early on it was recognized that LPPs should be constructed specifically for approximate OF-DFT functionals so that they could not only provide a much needed smooth electron-ion interaction potential, but they could also provide partially a correction to the

approximate KEDF potential<sup>14</sup>. These LPPs were soon abandoned<sup>23</sup> because the resulting LPPs had features that would induce numerical instability, would not lead to proper Coulomb decay of the LPP and, most importantly, were found to yield mixed results for condensed phases. So it seems we are at an impass, on one hand employing KS-DFT to build LPPs is likely to generate LPPs that are of little use in practical OF-DFT simulations where approximate KEDFs are used. On the other hand, building LPPs based on approximate KEDFs is associated with unmanageable side effects.

We also mention a notable recent approach, which involves evaluating directly the non-local part of the NLPP with orbital-free one-body reduced density matrices<sup>26</sup>. While the idea is promising, the resulting pseudopotentials are only accurate for a limited set of atoms, pointing to the fact that orbital-free formulations of reduced density matrices are often not N-representable<sup>27</sup>.

Considering the pros and cons of the various LPP design principles, in this work we aim to produce a library of LPPs for transition metal elements that can be used in conjunction with approximate KEDFs. The design principles adopted in this work arise from a careful formal analysis of atomic pseudization (carried out in the following section) and can be summarized with three points: (1) LPPs should target an *existing* set of NLPPs, (2) LPPs should differ from the NLPP's local part by a correction that is short ranged, and finally (3) LPPs should be constructed in conjunction with approximate KEDFs.

# II. AN IN-DEPTH LOOK AT PSEUDOPOTENTIALS AND PSEUDODENSITIES

In the PP approximation, the core electrons of each atom are represented by an effective nonlocal potential and the KS equations are only invoked for the valence electrons. The external potential becomes

$$v_{ext}(\mathbf{r}) \to v_{NLPP}(\mathbf{r}, \mathbf{r}') = v_{loc}(\mathbf{r})\delta(\mathbf{r} - \mathbf{r}') + v_{nl}(\mathbf{r}, \mathbf{r}')$$

$$\equiv v_{loc}(\mathbf{r}) + \hat{v}_{nl}$$
(5)

where we have indicated with a hat the nonlocal part of the NLPP.

NLPPs give rise to an electronic density  $n(\mathbf{r})$  (called pseudodensity) that only reflects the density of the valence electrons outside the core radii of the atoms and is smooth inside.

Such radii (NLPP cutoff radii, or  $R_{cut}^{nl}$ ) are parameters of the NLPPs and their value is determined by convenience. Small  $R_{cut}^{nl}$  will yield more accurate NLPPs but at the expense of needing to represent the more oscillatory components of the valence electrons.

The physical meaning of the nonlocal part of the NLPP is to maintain orthogonality between the valence and core orbitals. In KS-DFT,  $\hat{v}_{nl}$  is usually given in terms of a limited number of spherical harmonic projectors centered on the atoms.

#### A. Nonlocal Pseudopotential Representations

Once a particular NLPP is introduced, the solution of the KS equations yields a pseudodensity,  $n(\mathbf{r})$ . That same pseudodensity can be represented by many other NLPPs (hereafter indicated by  $\hat{v}_{NLPP}$ ). The usual map connecting external potentials with densities applies. However, this time we connect external, possibly nonlocal pseupotentials with a target pseudodensity

$$\hat{v}_{NLPP} \longrightarrow n(\mathbf{r}).$$
 (6)

Hohenberg and Kohn theorems for nonlocal external potentials due to Gilbert<sup>28</sup> apply and guarantee the existence of the above map, even though it is generally not bijective. The non-bijectivity is due to the fact that for a given choice of  $\hat{v}_{nl}$  one can find an associated  $v_{loc}(\mathbf{r})$  such that the KS equations yield the target density  $n(\mathbf{r})$ . Therefore there are multiple (potentially an infinite number) of  $\hat{v}_{NLPP}$  that have nonzero nonlocal part and that yield the same electron density,  $n(\mathbf{r})$ . We call the set of such NLPPs a NLPP representation. Typically, there is one NLPP having the property that beyond  $R_{cut}^{nl}$  not only the pseudodensity matches the all-electron density, but also the pseudo KS wavefunctions match the all-electron KS wavefunction for the isolated atom<sup>29</sup>.

The Hohenberg and Kohn theorems guarantee that if  $n(\mathbf{r})$  is noninteracting  $v_s$ -representable, then there is one and only one purely local PP (hereafter denoted by  $v_{LPP}(\mathbf{r})$ ) that, employed as external potential in the KS equations, yields the pseudodensity,  $n(\mathbf{r})$ . Namely, the bijective map

$$v_{LPP}(\mathbf{r}) \longleftrightarrow n(\mathbf{r})$$
 (7)

exists. We depict the concept of NLPP representation and the maps in Eqs. (6, 7) in Figure 1.

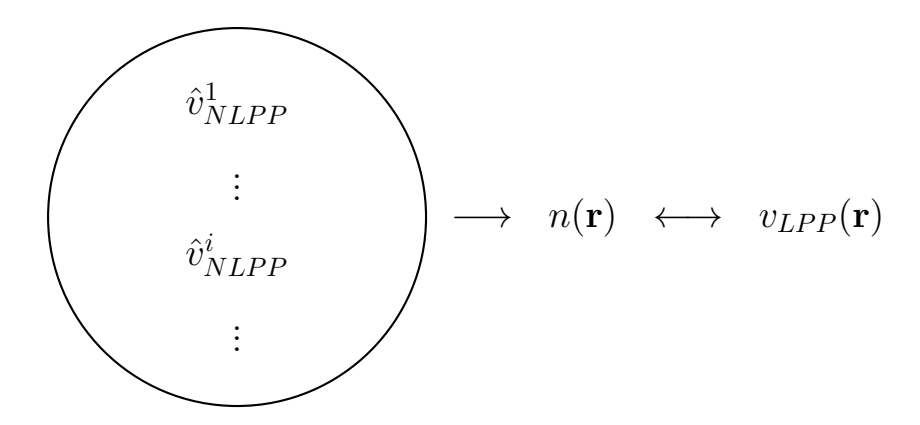


FIG. 1. Depiction of the maps in Eqs. (6,7) and the concept of NLPP representation (set of nonlocal PPs on the left-hand side) mapping to a target pseudodensity,  $n(\mathbf{r})$ . The bijectivity of the map connecting the pseudodensity with the associated local KS potential,  $v_{LPP}(\mathbf{r})$  is indicated by a left-right arrow.

The relation between the local PP,  $v_{LPP}(\mathbf{r})$ , and any of the NLPPs,  $\hat{v}_{NLPP}^{i}$ , can be derived on the basis of the optimized effective potential method (OEP)<sup>30,31</sup>, as we now explain.

### B. Relating Local and Nonlocal Pseudopotentials

We now seek to find the local PP,  $v_{LPP}(\mathbf{r})$ , that yields the target pseudodensity,  $n(\mathbf{r})$ . We first define the relevant energy functionals, one for a NLPP and one for a LPP,

$$E_{\hat{v}_{nl}}[n] = T_s^{\hat{v}_{nl}}[n] + E_{NL}^{\hat{v}_{nl}}[n] + E_{Hxc}[n] + \int v_{loc}^{\hat{v}_{nl}}(\mathbf{r})n(\mathbf{r})d\mathbf{r}$$

$$\tag{8}$$

$$E[n] = T_s[n] + E_{Hxc}[n] + \int v_{LPP}(\mathbf{r})n(\mathbf{r})d\mathbf{r}$$
(9)

where we have indicated with a superscript the quantities that are dependent on the choice of the purely nonlocal part of the NLPP, and we define the noninteracting kinetic energy in the NLPP case as

$$T_s^{\hat{v}_{nl}}[n] = -\frac{1}{2} \sum_i n_i^{\hat{v}_{nl}} \langle \phi_i^{\hat{v}_{nl}} | \nabla^2 | \phi_i^{\hat{v}_{nl}} \rangle \tag{10}$$

and the nonlocal energy,  $E_{NL}^{\hat{v}_{nl}}[n]$ ,

$$E_{NL}^{\hat{v}_{nl}} = \sum_{i} n_i^{\hat{v}_{nl}} \langle \phi_i^{\hat{v}_{nl}} | \hat{v}_{nl} | \phi_i^{\hat{v}_{nl}} \rangle = \text{Tr} \left[ \hat{v}_{nl} \hat{\gamma}_s^{\hat{v}_{nl}} \right]. \tag{11}$$

where  $\gamma_s^{\hat{v}_{nl}}$  is the KS density matrix of the NLPP KS system.

Crucially, we must require that  $E_{\hat{v}_{nl}}[n] = E[n]$ , Which delivers an important relation,

$$T_s^{\hat{v}_{nl}}[n] + E_{NL}^{\hat{v}_{nl}}[n] + \int v_{loc}^{\hat{v}_{nl}}(\mathbf{r})n(\mathbf{r})d\mathbf{r} = T_s[n] + \int v_{LPP}(\mathbf{r})n(\mathbf{r})d\mathbf{r}$$
(12)

which can be rearranged to

$$T_s^{\hat{v}_{nl}}[n] + E_{NL}^{\hat{v}_{nl}}[n] = T_s[n] + \int \Delta v_{LPP}(\mathbf{r}) n(\mathbf{r}) d\mathbf{r}.$$
(13)

In the above, we defined  $\Delta v_{LPP}(\mathbf{r}) = v_{LPP}(\mathbf{r}) - v_{loc}^{\hat{v}_{nl}}(\mathbf{r})$ , as the potential that achieves a KS inversion<sup>31–33</sup> of the NLPP KS system onto a LPP KS system.

Taking a functional derivative yields a crucial result

$$\Delta v_{LPP}(\mathbf{r}) = \frac{\delta T_s^{\hat{v}_{nl}}}{\delta n(\mathbf{r})} - \frac{\delta T_s}{\delta n(\mathbf{r})} + \frac{\delta E_{NL}^{\hat{v}_{nl}}}{\delta n(\mathbf{r})}$$
(14)

The above functional derivatives involve orbital-dependent functionals and thus can only be approached with OEP methods<sup>30</sup>. In the supplementary information document, we show how to apply OEP in this setting and we also show that  $\frac{\delta E_{NL}^{\hat{v}_{nl}}}{\delta n(\mathbf{r})}$  decays faster than the Coulomb interaction, specifically like a dipole field outside  $R_{cut}^{nl}$ .

In addition to  $\frac{\delta E_{NL}^{\hat{v}_{nl}}}{\delta n(\mathbf{r})}$ , let us also consider the  $\frac{\delta T_s^{\hat{v}_{nl}}}{\delta n(\mathbf{r})} - \frac{\delta T_s}{\delta n(\mathbf{r})}$ , a term which is more challenging in nature. This is because the NLPP and LPP KS orbitals are generally different and would not yield the same kinetic energy unless the wavefunctions coincide beyond a radial cutoff<sup>34</sup>. We note that PPs are derived to maintain the Coulomb tail behavior beyond a certain cutoff radius, which we shall indicate by  $R_{cut}^{Coul}$ . Eq. (14) shows us that the local parts of the NLPP should be equal to the LPP beyond the larger of the  $R_{cut}^{Coul}$  among NLPP and LPP, ensuring that  $\Delta v_{LPP}(\mathbf{r}) = 0$  beyond this cutoff radius.

Unfortunately, there is generally no guarantee that  $R_{cut}^{Coul}$  for the LPP KS system will be small. However, early work<sup>25</sup>, pioneering work by Mi et al.<sup>18</sup>, as well as more recent studies from the Huang group<sup>17</sup>, demonstrate that for several transition metals,  $R_{cut}^{Coul}$  can be made as small as typical cutoff radii used in standard pseudopotentials.

Thus, we should expect to be able to construct LPPs for a significant set of transition metal elements. This is a quest we tackle head-on in the next sections.

# III. SIMULTANEOUSLY APPROXIMATING $\Delta v_{LPP}(\mathbf{r})$ AND THE OF-DFT OEP PROBLEM

We now change gears as we consider approximate KEDFs, indicated by  $\tilde{T}_s$ , typically employed in OF-DFT simulations. All expressions derived thus far apply only to systems where an exact  $T_s$  functional is used. Taking  $\Delta v_{LPP}(\mathbf{r})$  from Eq. (14) from the previous section, we can now reformulate it to also correct for approximate KEDFs as follows,

$$\Delta v_{LPP}(\mathbf{r}) = \frac{\delta T_s^{\hat{v}_{nl}}}{\delta n(\mathbf{r})} - \frac{\delta \tilde{T}_s}{\delta n(\mathbf{r})} + \frac{\delta E_{NL}^{\hat{v}_{nl}}}{\delta n(\mathbf{r})}.$$
 (15)

This definition clearly shows two goals for  $\Delta v_{LPP}(\mathbf{r})$ : (1) it includes the effect of the nonlocal part of the KS-DFT PP; (2) it corrects for the fact that KEDFs are approximate, making sure that the density of the OF-DFT system matches the one of the KS-DFT system. Hence, the selection of the KEDF is based on computationally efficient functionals shuch as TF+vW. Thus, the result of approximating  $\Delta v_{LPP}(\mathbf{r})$  is to simultaneously achieve the two goals.

To approximate it, we first impose it to be spherically symmetric around each ion, i.e.,  $\Delta v_{LPP}(\mathbf{r}) \equiv \Delta v_{LPP}(r)$ , with  $r = |\mathbf{r} - \mathbf{R}_I|$  for  $\mathbf{r}$  in the vicinity of ion I, where  $\mathbf{R}_I$  is the position of the I-th ion. Then, we impose the following boundary conditions that ensure smoothness and short rangedness, with  $r_{cut}$  being a user defined cutoff radius,

$$\begin{cases} \Delta v_{LPP}(r) = 0 & \text{if } r = r_{cut}, \\ \frac{d\Delta v_{LPP}(r)}{dr} = 0 & \text{if } r = r_{cut} \text{ and } r = 0. \end{cases}$$
(16)

We choose a polynomial ansatz

$$\Delta v_{LPP}(r) = a_0 + a_1 d(r) + a_2 d(r)^2 + a_3 d(r)^3 + a_4 d(r)^4 + a_5 d(r)^5$$
(17)

where  $d(r) = r - r_{cut}$ . After applying the conditions above, we find  $a_0$  and  $a_1$  to vanish, and  $a_2 = 3a_3r_{cut} - 4a_4r_{cut}^2 + 5a_5r_{cut}^3$ . The remaining three parameters  $(a_3, a_4 \text{ and } a_5)$  are optimized minimizing the following cost function (exposing the dependence of the densities on the pseudopotentials),

$$\Delta n = \frac{1}{2} \int |n_{OF}[v_{LPP}](\mathbf{r}) - n_{KS}[\hat{v}_{NLPP}](\mathbf{r})| d\mathbf{r}, \qquad (18)$$

where

$$n_{OF}(\mathbf{r}) = \arg\min_{n} \left\{ \tilde{T}_s[n] + E_{Hxc}[n] + \int v_{LPP}(\mathbf{r}) n(\mathbf{r}) d\mathbf{r} \right\}$$
(19)

and  $n_{KS}(\mathbf{r})$  is the KS-DFT pseudodensity arising from a particular choice of nonlocal PP. The minimization effectively, yet approximately, implements OEP because the loss function is minimum when the OF-DFT density is close to the KS-DFT pseudodensity.

Important aspects to note are that  $\Delta v_{LPP}(\mathbf{r})$  is: (1) short ranged around each ion, as it is only nonzero for  $0 \leq |\mathbf{r} - \mathbf{R}_I| \leq r_{cut}$ ; (2) of spherical symmetry around each ion. Thus, the resulting LPP, given by  $v_{loc}^{\hat{v}_{nl}}(r) + \Delta v_{LPP}(r)$  maintains the correct Coulomb decay in agreement with the target NLPP. Finally, we note that there is freedom in choosing the cutoff radii  $(r_{cut})$ . We use the value of the largest of the  $R_{cut}^{nl}$  of the target NLPP, see supplementary Table S1. We will see in the results section that this choice might not be the most optimal given the restrictive, polynomial ansatz for  $\Delta v_{LPP}(r)$ . The choice of cutoff radius will deserve further consideration in future works.

Regarding the choice of polynomial ansatz for  $\Delta v_{LPP}(r)$ , after testing, we found that a 5th order provides a good balance between accuracy of teh LPPs and computational cost of the LPP optimizer. Reducing the order of the polynomial would result is significantly lower quality LPPs, and increasing the order would result is significant computational cost and convergence complexity for the optimizer.

#### IV. COMPUTATIONAL DETAILS

The KS-DFT calculations were performed using the Python package QEpy<sup>35</sup>, which is interfaced with Quantum Espresso (QE)<sup>36</sup>. All simulations employed a Monkhorst-Pack grid<sup>37</sup> of  $11 \times 11 \times 11$  k-points and a plane wave cutoff energy of 680 eV for the wavefunctions (four times as much for the electron pseudodensity). We chose two nonlocal, ultrasoft PPs, namely, GBRV<sup>38</sup> and PSL<sup>39</sup> due to their ability to retain accuracy across the periodic table while maintaining a workable plane wave cutoff. The KS-DFT calculations were run with these PPs while the OF-DFT calculations were ran with either only the local part of the PPs or with the additional  $\Delta v_{LPP}(\mathbf{r})$  correction discussed before.

The OF-DFT calculations were carried out using the DFTpy Python package<sup>40</sup> with a plane wave cutoff energy of 1600 eV. To compare to existing LPPs for OF-DFT simulations, we employed the High-Quality Local Pseudopotentials (HQLPP) of recent conception<sup>17</sup>.

All calculations employed the Local Density Approximation (LDA) xc functional proposed by Perdew and Zunger<sup>41</sup>. Therefore, target results in this work are given by pseudopotential KS-DFT simulations employing the LDA functional. We also tested our pseudization procedure using PBE<sup>2</sup> for Ag recovering a similarly accurate pseudization as LDA (see Results section). Testing other xc functionals will be matter of future work.

Unless otherwise stated, bulk calculations are carried out on the primitive cell of the most stable phase, the equation of state (EOS) curves were generated by varying the lattice parameter from  $0.9V_0$  to  $1.2V_0$ , where  $V_0$  is the equilibrium volume. From these curves, the minimum energy  $(E_0)$  and bulk modulus  $(B_0)$  were obtained by fitting the energy versus volume data to Murnaghan's equation of state<sup>42</sup>. We further assess the transferability of the new pseudopotentials using a nonlocal KEDF, revHC<sup>43</sup>, for the EOS parameters. To observe the effects of xc on the construction of the new pseudopotentials we included in the Supplementary Information Tables S10-S12 the EOS parameters of Ag with the functional Perdew-Burke-Ernzerhof<sup>2</sup> (PBE) xc.

Phonon spectra calculations were performed using experimental lattice constants and different methods for KS-DFT and OF-DFT. For KS-DFT, the phonon calculations were conducted in QE using Density Functional Perturbation Theory<sup>44,45</sup>. For OF-DFT, the DFTpy package was used as a calculator within the Atomic Simulation Environment (ASE) Python package to compute phonons via finite differences, employing  $5 \times 5 \times 5$  supercells. Due to the low computational cost of OF-DFT simulations with DFTpy<sup>46</sup>, the OF-DFT phonon calculations did not add a significant overhead.

Isolated atom calculations were performed by placing one atom in a cubic cell with a side length of 15 Å.

#### V. RESULTS AND DISCUSSION

The new set of pseudopotentials generated by the procedure in Section III are termed PGBRV1.0, PPSL1.0, PGBRV0.2, and PPSL0.2 where the prepending "P" represents the pseudization for OF-DFT, PSL and GBRV represent the reference KS NLPP used, and the digits represent the kind of KEDF used to build  $\Delta v_{LPP}$ . We employed the Thomas-Fermi (TF) plus von Weizsäcker (vW) functional with 100% vW (1.0) or 20% vW (0.2).

In the following sections, we analyze the performance of the new set of pseudopotentials for transition metal elements. We first analyze the electron density of periodic systems and assess the ability of the new LPPs to reproduce the KS-DFT reference density of the most stable phase of transition metals. We also show that the new LPPs are applicable to several crystal phases not only the ones used for the PP development. We then move to analyze the electron density of isolated atoms to infer on the applicability of the PPs in combination with approximate KEDFs. For selected elements, we also test phonon spectra and an analysis of the electron density for cluster systems.

#### A. Generation of the new LPPs

The LPPs are generated according to Eqs. (16–19) for all transition metals. Inspired by BLPs<sup>23</sup>, we pseudized atoms in the condensed phase, choosing the most stable phases for each of the elements employing the experimental lattice constants.

The success of the pseudization is given by how well the density difference between the target KS-DFT,  $n_{KS}[\hat{v}_{NLPP}]$ , and the OF-DFT,  $n_{OF}[v_{LPP}]$ , pseudodensities in Eq. (18) can be minimized as a function of the parameters (a to e in Eq. (17)) defining the LPP correction,  $\Delta v_{LPP}(r)$ . We choose the percentage density deviation,  $\Delta_v$ , as a measure of success,

$$\Delta_v = 100 \times \frac{\Delta n}{N_v} \tag{20}$$

where  $N_v$  is the number of valence electrons. We note that  $\Delta n \leq N_v$ , thus  $\Delta_v \leq 100$ . In the Supplementary material (Figure S1) we show the spatial distribution of the electron density difference between the OF and KS in a representative cut plane of the most stable phases for Ag, Cu, Pd, and Mo, to validate the convergence criteria in Eq. (20).

Figure 2 provides a visual showing three sets: the color green, red, and blue; green highlights elements where the new pseudopotentials have  $\Delta_v$  lower than 5%, red elements have  $\Delta_v$  between 5% and 8%, and blue elements have  $\Delta_v$  greater than 8%. The figure clearly shows that PGBRV LPPs generally yield pseudodensities closer to the KS reference compared to the other LPPs. We note that the pseudization dramatically improves upon the densities determined using directly the local part of the NLPP (i.e.,  $v_{loc}^{\hat{v}_{nl}}$ ) which show an erratic behavior with often very inadequate  $\Delta_v$  values. This is an important result as using the local part of the NLPP is a common practice in OF-DFT whenever accurate LPPs are not available<sup>47</sup>.

We observed that for those elements where the local part of the NLPP already provides pseudodensities  $\sim 15\%$  deviated from the KS-DFT reference, minimization of Eq. (18) is

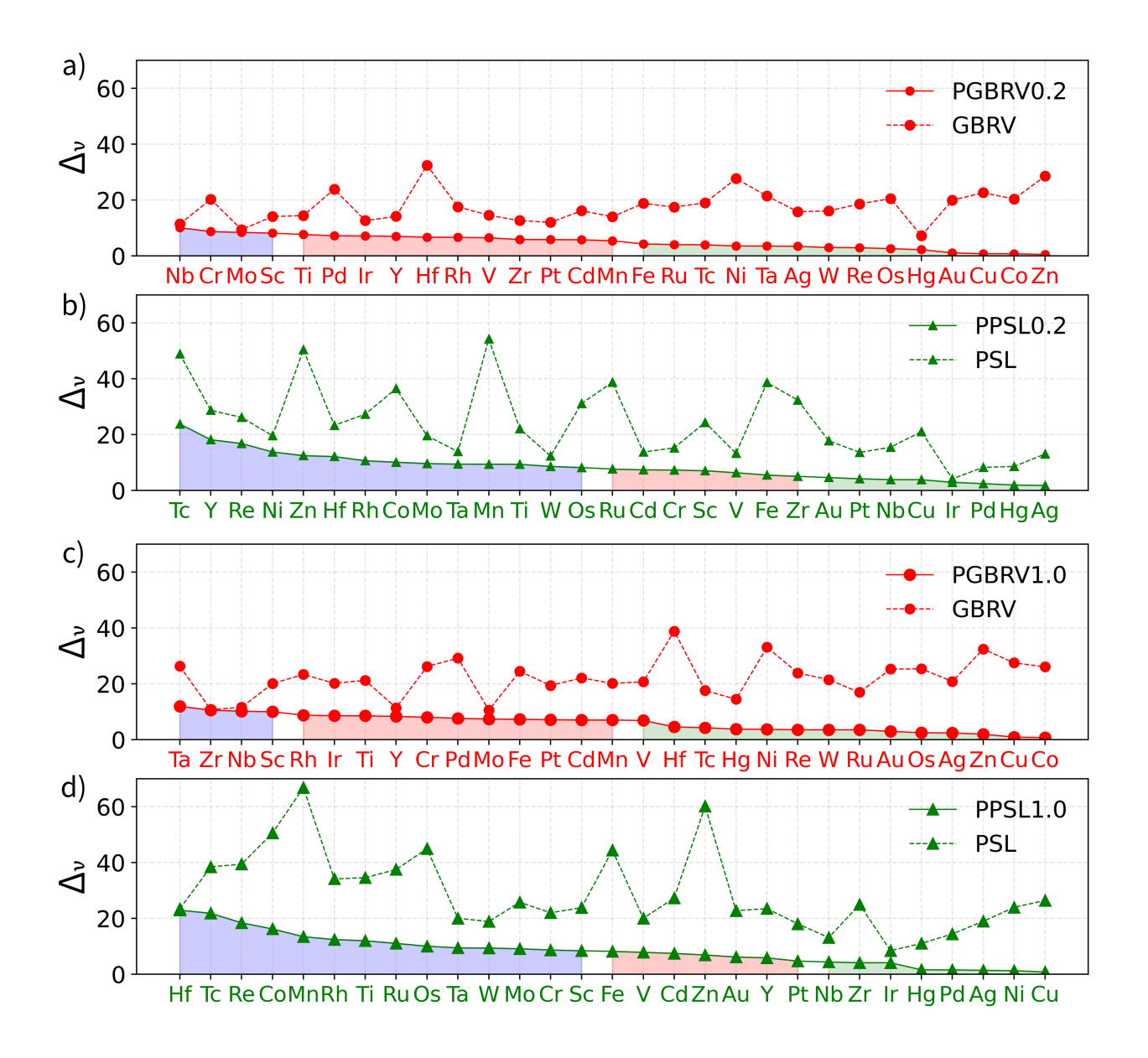


FIG. 2. Percent density deviation,  $\Delta_v$ , for the atoms in the most stable phase of all transition metals. Green regions are elements with  $\Delta_v \leq 5\%$ ; red  $5 < \Delta_v \leq 8\%$  and blue  $\Delta_v > 8\%$ . The four panels are each devoted to one set of pseudopotentials (PGBRV0.2, PGBRV1.0, PPSL0.2, PPSL1.0, see text for more details).

challenging. We observed this to be the case for Nb, Mo, and Hg for PGBRV0.2, and Zr, Nb, Y, and Mo for PGBRV1.0.

When comparing PGBRV0.2 (PGBRV1.0) with PPSL0.2 (PPSL1.0), we observe that elements pseudized well by one are often less effectively pseudized by the other. Our analysis suggests this behavior stems from differences in the cutoff radii of the two NLPPs, which

directly affect the domain of the polynomial defined in Eq. (17). Specifically, as illustrated in supplementary Table S1 and the EOS results in Tables S2-S5, when the GBRV  $R_{cut}^{nl}$  is larger than that of PSL (e.g., for Nb), PPSL0.2 [recalling our choice  $r_{cut} = \max(R_{cut}^{nl})$  in Eq. (17)] results in smaller density deviations compared to PGBRV0.2. Conversely, for elements such as Ni, Re, Zn, Ta, and W, the smaller GBRV  $R_{cut}^{nl}$  yields more accurate pseudization with PGBRV0.2 than with PPSL0.2. Similarly, PGBRV1.0 pseudopotentials outperform PPSL1.0 for Re and W, while PPSL1.0 provides better results for Zr. These observations underscore the significance of  $r_{cut}$  in defining LPPs, suggesting that the optimal choice of cutoff radius should be element-specific and optimized.

In sum, PGBRV0.2 and PGBRV1.0 LPPs provide a better pseudization than PPSL0.2 and PPSL1.0. Elements successfully pseudized by PGBRV0.2 and PGBRV1.0 are Co, Cu, Zn, Os, Ni, Ag, Au, Re, W, Hg, Ru, and Tc, while for Pd, Cd, V, Mn, and Pt the pseudization is moderately successful. Nb, and Sc are consistently difficult elements for both TFvW and TF0.2vW functionals and NLPPs.

To understand (and predict) the quality of the pseudization, we consider the density displacement presented just now but we order the data by element group and split the data for the three transition metal periods. We also change slightly the plotted indicator to the density deviation relative to the number of d-electrons (rather than valence electrons, see Figure 3), which we define as follows

$$\Delta_d = 100 \times \frac{\Delta n}{N_d} \tag{21}$$

where  $\Delta n$  is defined in Eq. (18), and  $N_d$  is the number of valence d-electrons.  $\Delta_d$  normalizes  $\Delta n$  differently from Eq. (20). Specifically,  $N_v$  includes semicore electrons while  $N_d$  only includes valence d electrons. Some elements may be pseudized differently by the GBRV and PSL NLPPs. For example Ag with GBRV has 4s and 4p semicore electrons (total of 8) while PSL includes no semicore electrons in the pseudodensity of this element.

A general trend arises from Figure 3:  $\Delta_d$  varies monotonically along the transition metal rows. That is, for late transition metals (e.g., Cu, Zn, Ag, Cd, Au, and Hg) both types of LPPs converge to similar, low  $\Delta_d$  values indicating good pseudization. In contrast, early transition metals (e.g., Sc, Ti, and Y) exhibit larger displacements for both LPPs. We interpret this behavior noticing that KEDFs are known to perform better as the number of electrons increases, consistent with the exactness of the Thomas-Fermi functional in the

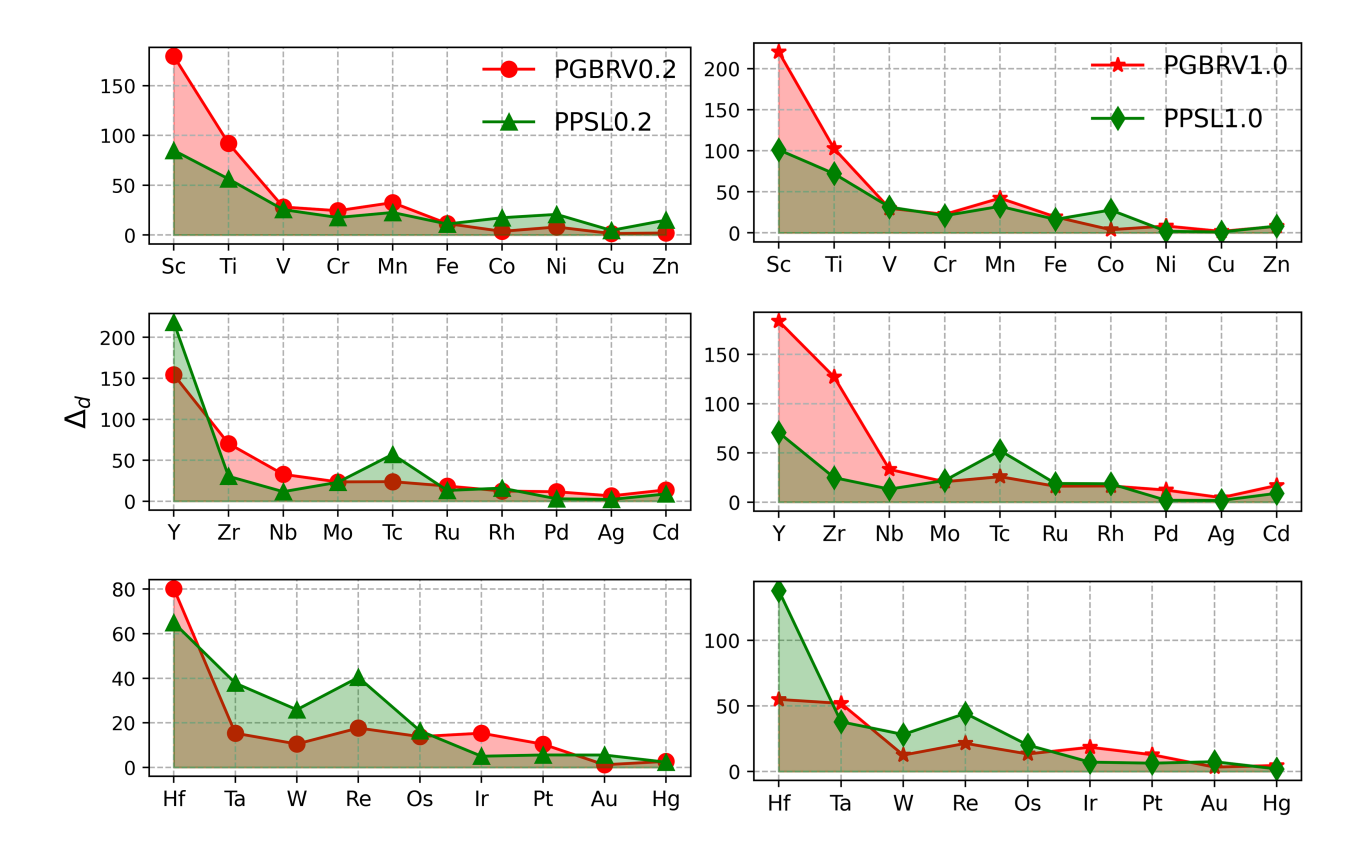


FIG. 3. Density deviation per d electron,  $\Delta_d$ . The panels compare pseudopotentials constructed using the TF0.2vW functional (left) and the TFvW functional (right) for transition metals. Red circles represent GBRV pseudopotentials, green triangles PSL.

limit of an infinite electron system<sup>48</sup>.

We also observe considerable variability in results for group 3–5 transition metals, independent of the period. For example, the PGBRV pseudopotentials yield higher displacements for Sc and Ti compared to PPSL, whereas for Y, PPSL1.0 performs best, followed by PPSL0.2 and then the PGBRV LPPs. While the exact reasons for this behavior remain unclear (we note that GBRV and PSL pseudize each of Y, Sc and Ti with the same number of valence electrons), as noted before it likely relates to the different  $r_{cut}$  values employed in these LPPs. For Y, GBRV uses  $r_{cut} = 2.2 a_0$ , while PSL uses  $r_{cut} = 1.8 a_0$ . This highlights the need for a follow-up study focused on optimizing  $r_{cut}$  for these new pseudopotentials. Although we have adopted  $r_{cut}$  values from the original NLPPs, more suitable choices may exist.

### B. Equation of State

From the previous analysis, we have chosen to further investigate PGBRV0.2 for a selected set of atoms such as Cu, Ag, and Pd for which PGBRV0.2 is expected to improve upon the local part of the GBRV PP (i.e., the  $v_{loc}^{\hat{v}_{nl}}$  mentioned before). We also present Mo for which we predict the PGBRV0.2 will not provide improved electronic structure compared to the local part of the GBRV NLPP. The analysis involves computation of EOS parameters (equilibrium volume,  $V_0$ ; equilibrium energy,  $E_0$ ; and bulk modulus,  $E_0$ 0 for FCC, BCC, and HCP phases. We compare the PGBRV0.2 results with the local part of the GBRV NLPP and HQLPP. All calculations are carried out with TF0.2vW and the nonlocal revHC KEDFs. The results are collected in Tables I for Ag, II for Cu, III for Pd, and IV for Mo, where we show the relative error of  $V_0$  and  $E_0$ 0 and the energy difference compared to the most stable phase of the presented elements. The EOS parameters from KS (LDA) are compared to experimental values as shown in Table S9 and show that the KS-DFT benchmark results are close to experimental ground truth for lattice constants and within 30% for bulk moduli.

Generally, we notice that PGBRV offers an improved description compared to the local part of GBRV regardless of the functional employed. In comparison to HQLPP, the PGBRV LPPs generally perform better. For example, they provide better  $V_0$  and better  $B_0$ . This is true generally except perhaps for Mo. We notice that for Mo the  $\Delta_v$  metric for pseudization did not show any improvement compared to the local part of GBRV (see panel (a) of Figure 2).

Analyzing the specifics, we see that while the EOS parameters values for either TF0.2vW or revHC are not quantitative, they recover important trends for the equilibrium volume (even though it is generally underestimated by about 10-30%) as well as the bulk modulus. For the latter, we note that approximate KEDFs generally struggle to produce qualitative bulk moduli. However, despite the large deviation, we can discern a generally recovered trend. For example, HCP  $B_0$  is systematically larger than the FCC or BCC  $B_0$ . The energy ordering of the phases is also generally recovered with FCC consistently predicted to be the most stable phase.

Even though the results presented in Tables I–IV, as well as in supplementary Tables S2-S5, are not quantitatively accurate, they are nonetheless reasonable. In Table S6 we show an statistical summary of Tables S2-S5, where the Mean Absolute Relative Error (MARE)

values ( $\approx 50-60\%$ ) obtained for  $V_0$  and  $B_0$  using the original GBRV and PSL pseudopotentials indicate high discrepancies between the OF-DFT and KS-DFT frameworks. In contrast, the new local pseudopotentials (PGBRV0.2 and PPSL0.2) significantly reduce the MARE for  $V_0$  to 28–37%, corresponding to a significant improvement in accuracy relative to emplying the local part of the KS-DFT pseudopotentials. Although the  $B_0$  values remain less accurate (MARE  $\approx 55-60\%$ ), all materials are predicted to be bound. This results are nontrivial for OF-DFT calculations<sup>49,50</sup>, and as previously noted, the OF-DFT calculations employing the newly developed LPPs successfully capture several trends observed in the KS-DFT EOS parameters. To rationalize this outcome, we emphasize that the PGBRV0.2 LPP is designed not only to partially recover effects associated with the nonlocal component of the NLPP, but also, crucially, to locally invert the KS density in regions near the ionic cores. Consequently, using the PGBRV0.2 pseudopotentials yields electron densities of substantially higher quality than would be obtained using a generic, KEDF-agnostic LPP. A clear demonstration of this point is provided by the performance comparison with HQLPP pseudopotentials, which yield lower accuracy than PGBRV0.2 a more detailed quantitative comparison between PGBRV0.2 and HQLPPs performance is provided in Tables S7 of the Supplementary Information. Upon switching to the revHC functional (Table S8), the PG-BRV0.2 potentials maintain comparable accuracy (MARE  $\approx 20-40\%$ ), while the HQLPPs exhibit larger deviations. These results confirm that the new pseudopotentials achieve improved consistency with KS-DFT and remain transferable across different KEDFs. This discrepancy does not reflect a flaw in the HQLPP pseudopotentials, as they were explicitly constructed to best represent electron densities calculated with the exact KEDF.

### C. Phonons

Figure 4 shows the phonon spectra for the noble metals in their FCC phase (Cu, Ag, and Au) as well as Pd also in the FCC phase calculated with TF0.2vW and two LPPs: the local part of GBRV and PGBRV0.2. The reference KS-DFT with GBRV NLPP is also included. Despite noticing a general underestimation, phonon dispersions produced by PGBRV0.2 are in good agreement with KS-DFT results and are seen to improve dramatically on the results from using the LPP from the local part of the GBRV NLPP.

From the previous sections we found that although Pd is an element that does not reach

TABLE I. Percentage errors in the equation of state parameters for  $V_0$  and  $B_0$  with respect to KS-DFT results, and energy difference against the stable phase  $E_0$  of Ag. A dash — indicates that the phase is found to be unbound.

Ag	Functional	PP	$V_0$	$E_0$	$B_0$
			(%)	(eV/atom)	(%)
	KS	GBRV	0.00	-4023.32	0.00
	TF0.2vW	GBRV	43.0	-3719.80	44.6
7)		PGBRV0.2	20.1	-4546.42	22.3
FCC		HQLPP	34.7	-4054.91	50.4
		GBRV	58.1	-3731.58	56.8
	revHC	PGBRV0.2	13.3	-4380.85	12.2
		HQLPP	22.6	-3998.92	50.4
	KS	GBRV	0.00	0.01	0.00
	TF0.2vW	GBRV	35.8	0.14	59.5
Ο.		PGBRV0.2	17.2	0.04	30.1
HCF		HQLPP	33.9	0.01	66.5
	revHC	GBRV		_	
		PGBRV0.2	14.1	0.01	27.7
		HQLPP	19.0	0.01	35.8
	KS	GBRV	0.00	0.04	0.00
	TF0.2vW	GBRV	42.8	0.05	45.7
BCC		PGBRV0.2	20.7	0.04	25.4
		HQLPP	34.7	0.00	49.3
	revHC	GBRV		_	
		PGBRV0.2	14.4	0.0	10.1
		HQLPP	34.5	-0.02	55.8

high convergence in its pseudization, we found PGBRV0.2 still delivered physical EOS parameters. For this reason, we show its phonon spectrum in the last panel of Figure 4. We note that Pd phonons computed with the PGBRV0.2 LPP are once again much improved

TABLE II. Percentage errors in the equation of state parameters for  $V_0$  and  $B_0$  with respect to KS-DFT results, and energy difference against the stable phase  $E_0$  of Cu. A dash — indicates that the phase is found to be unbound.

Cu	Functional	PP	$V_0$	$E_0$	$B_0$
			(%)	(eV/atom)	(%)
	KS	GBRV	0.00	-5490.58	0.00
		GBRV	81.0	-4613.32	63.5
FCC	TF0.2vW	PGBRV0.2	11.5	-6947.80	56.1
		HQLPP	78.5	-5599.68	73.5
		GBRV	115.0	-4625.80	66.7
	revHC	PGBRV0.2	27.2	6979.97	75.7
		HQLPP			
	KS	GBRV	0.00	0.02	0.00
	TF0.2vW	GBRV			_
Ο.		PGBRV0.2	8.8	0.01	55.8
HCP		HQLPP	103.2	0.02	94.4
	revHC	GBRV		_	
		PGBRV0.2	8.3	-0.038	56.7
		HQLPP	84.4	-5483.58	52.8
	KS	GBRV	0.00	0.05	0.00
	TF0.2vW	GBRV	81.3	0.02	64.5
BCC		PGBRV0.2	11.1	0.01	55.9
		HQLPP	116.3	0.00	98.4
	revHC	GBRV	144.0	0.07	86.6
		PGBRV0.2	24.8	0.00	73.7
		HQLPP			

compared to using the local part of the GBRV NLPP. In the supplementary materials we show the phonon dispersion of Mo and Zr where the local part of GBRV produces several imaginary frequencies, PGBRV0.2 does not. Although for these elements the comparison

TABLE III. Percentage errors in the equation of state parameters for  $V_0$  and  $B_0$  with respect to KS-DFT results, and energy difference against the stable phase  $E_0$  of Pd. A dash — indicates that the phase is found to be unbound.

Pd	Functional	PP	$V_0$	$E_0$	$B_0$
			(%)	(eV/atom)	(%)
	KS	GBRV	0.00	-2704.79	0.00
	TF0.2vW	GBRV	68.8	-2336.16	69.7
		PGBRV0.2	14.5	-2929.42	61.8
FCC		HQLPP	55.2	-3544.12	76.3
		GBRV	51.6	-2343.41	51.3
	revHC	PGBRV0.2	25.2	-2927.97	7.9
		HQLPP	31.5	-3488.77	71.5
	KS	GBRV	0.00	0.03	0.00
	TF0.2vW	GBRV	58.8	0.20	84.6
0.		PGBRV0.2	11.0	0.00	59.2
HCP		HQLPP	43.6	.01	68.9
	revHC	GBRV	45.2	0.061	66.3
		PGBRV0.2	26.4	-0.006	13.9
		HQLPP	_		
	KS	GBRV	0.00	0.05	0.00
	TF0.2vW	GBRV	67.7	0.02	67.3
BCC		PGBRV0.2	14.1	0.02	60.5
		HQLPP	52.4	0.00	73.2
	revHC	GBRV	47.8	-0.08	43.6
		PGBRV0.2	26.6	0.00	14.1
		HQLPP	22.0	0.00	60.9

with KS-DFT is not as clean as for the noble metals or Pd, the improved phonon dispersion of PGBRV0.2 vs local part of GBRV is still quite clear. These observations are consistent with our analysis of the pseudization in section VA, Zr is the worst performer.

TABLE IV. Percentage errors in the equation of state parameters for  $V_0$  and  $B_0$  with respect to KS-DFT results, and energy difference against the stable phase  $E_0$  of Mo. A dash — indicates that the phase is found to be unbound.

Мо	Functional	PP	$V_0$	$E_0$	$B_0$
			(%)	(eV/atom)	(%)
	KS	GBRV	0.00	-1897.97	0.00
	TF0.2vW	GBRV	22.3	-2140.32	72.4
7)		PGBRV0.2	38.1	-1990.97	74.8
BCC		HQLPP	40.9	-1906.13	77.3
		GBRV	3.2	-2145.08	47.9
	revHC	PGBRV0.2	19.7	-1994.48	62.2
		HQLPP	11.3	-1863.92	9.8
	KS	GBRV	0.00	0.43	0.00
	TF0.2vW	GBRV	20.4	-0.02	69.6
(۲		PGBRV0.2	34.7	0.04	74.5
FCC		HQLPP	38.4	0.00	74.1
	revHC	GBRV	2.3	0.11	45.6
		PGBRV0.2	19.9	0.00	59.3
		HQLPP	11.8	0.01	5.7
	KS	GBRV	0.00	0.44	0.00
		GBRV	17.2	0.01	69.6
HCP	TF0.2vW	PGBRV0.2	30.0	0.04	73.7
		HQLPP	36.9	0.00	78.2
	revHC	GBRV	1.5	0.02	56.4
		PGBRV0.2	18.5	0.0	65.7
		HQLPP	12.1	0.0	23.4

## D. Compatibility of KEDF/LPP combinations

To evaluate the compatibility and performance of the proposed LPPs with several KEDF approximants, we examine the electron density of isolated atoms between two classes of

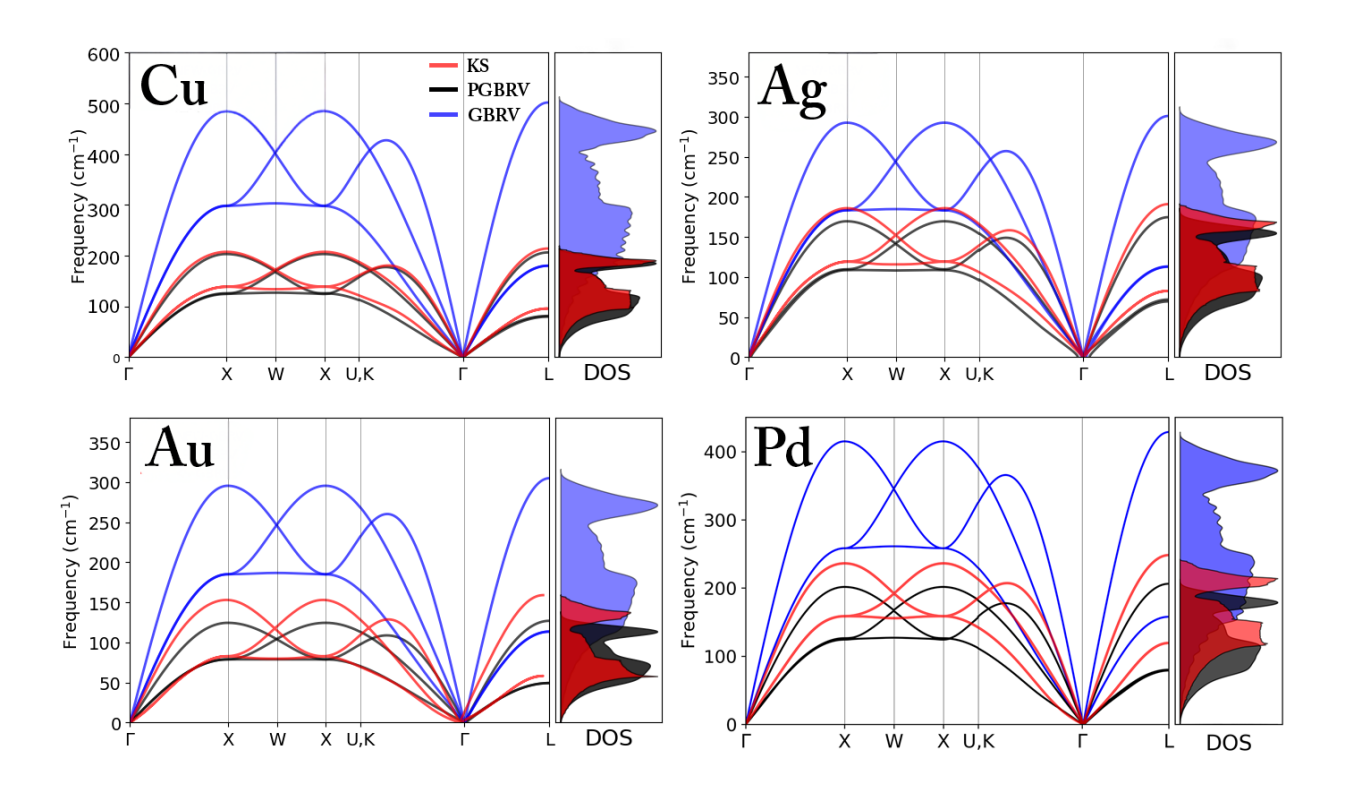


FIG. 4. Phonon spectra of Cu, Ag, Au, and Pd calculated with OF-DFT using TF0.2vW with PGBRV0.2 LPPs (black lines) and the local part of the GBRV NLPPs (blue lines). Reference KS-DFT are also included (red line).

KEDFs: semilocal (LKT<sup>51</sup>, revAPBEK<sup>48</sup>) and nonlocal (LMGP and revHC) KEDFs in comparison with densities computed with either TF0.2vW or TFvW employing the new LPPs, see Figure 5. To better understand the results for semilocal KEDFs, we consider the enhancement factor, F(s), as a function of the reduced density gradient,  $s(\mathbf{r})$ . Further details on the explicit forms of F(s) for the different semilocal KEDFs discussed here (TFvW, TF0.2vW, LKT, and revAPBEK) are provided in the Supplementary Information section II. The left most panel of Figure 5 shows F(s) where we notice that for small values of  $s(\mathbf{r})$ , where the electron density is usually large LKT, revAPBEK, and TFvW have a noticeably higher F(s) compared to TF0.2vW. The enhancement factor for TF0.2vW, due the small vW prefactor of 0.2, displays a slower upward behavior compared to the other functionals. Similarly for large values of  $s(\mathbf{r})$ , which correspond to diffuse or tail regions of the density, the enhancement factor increases significantly for TFvW and LKT while it remains low for TF0.2vW and revAPBEK. The latter is due to its asymptotic behavior<sup>51</sup>. This analysis shows that LKT, revAPBEk and TFvW are likely more compatible with densities form

TFvW in conjunction with PGBRV1.0 and PPSL1.0 than with densities from TF0.2vW in conjuction with PGBRV0.2 and PPSL0.2.

The two histograms of  $\Delta n_{\rm iso}$  (defined in Eq. (18) bit applied to isolated atoms) in Figure 5 clearly show that nonlocal functionals yield densities closer to TF0.2vW (with PGBRV0.2) with an average deviation of 0.5e. In contrast, these functionals against TFvW (with PGBRV1.0) show an average deviation of 1.4e. Semilocal functionals show an opposite behavior deviating by 1.0e from TF0.2vW and a meager 0.25e for TFvW.

Overall, these results emphasize the importance of internal consistency between the chosen LPP and the KEDF, particularly when applying OF-DFT to systems characterized by large density gradients or strong localization effects. This compatibility issue between KEDF and LPP was seen as a negative aspect by some<sup>23</sup>. However, in the context of this work, we see that already the two functionals considered for LPP construction, TFvW and TF0.2vW, form an excellent platform or "basis set" of KEDFs to be able to accommodate an array of functionals. Should one require a functional-specific LPP, the option to follow the LPP construction workflow presented here is always available and achievable using the software provided in the supplementary information document.

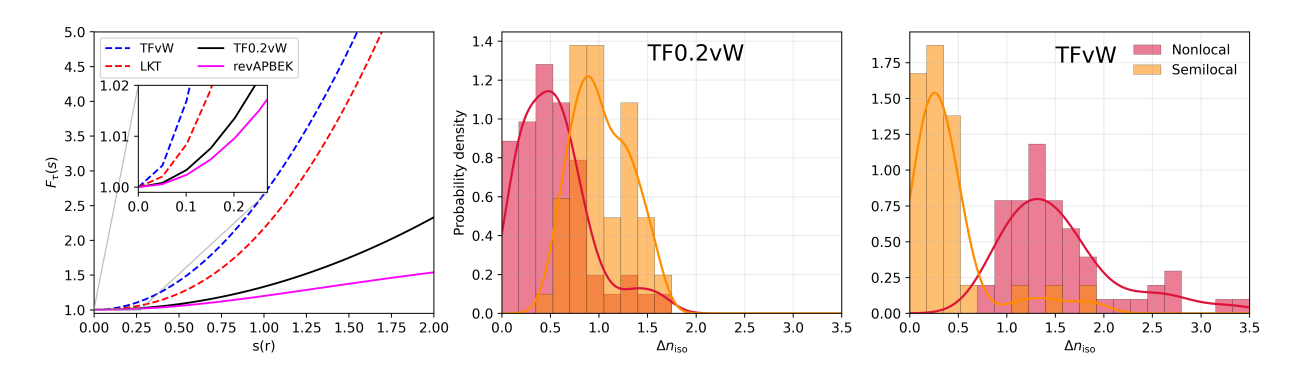


FIG. 5. Left-most panel: enhancement factor,  $F_{\tau}(s)$ , of several GGA functionals. Right two panels: electron density deviation,  $\Delta n_{iso}$ , against TF0.2vW and TFvW functionals for several GGA KEDF (LKT, revAPBEk, TFvW) and nonlocal functionals (revHC and LMGP).

#### E. Clusters

In this section, we evaluate the performance of the new PGBRV0.2 LPPs in describing the electronic density of finite systems. Specifically, we study Pd<sub>13</sub>, Ag<sub>20</sub>, and Pt<sub>10</sub> clusters (for

PPSL see supplementary Tables S6-S8). The electronic density difference,  $\Delta n$ , is computed as in Eq. (18). From the results, we observe that the electron density calculated with the PGBRV0.2 LPPs is in generally good agreement with KS electron density, showing an error of 10% or less.

The best performers are LMGP for  $Pd_{13}$  (7.3% deviation), LKT for  $Ag_{20}$  (3.8% deviation) and TF0.2vW for  $Pt_{10}$  (6.1% deviation). When averaging over all three clusters, the TF0.2vW functional yields the smallest overall electron density difference ( $\Delta n/N_v = 0.059$ ), thus representing the best overall performer in this set, followed closely by revHC (0.064), LMGP (0.075), LKT (0.085) and lastly TFvW (0.105). The results also show that the electron density is always improved (up to 79% improvement!) compared to using the local part of the GBRV NLPP.

TABLE V. Relative density difference (against KS) for Pd<sub>13</sub>. The OF-DFT electron density is computed with the local part of the GBRV NLPP as well as with PGBRV0.2. Improvement (%) indicates the percent improvement of the PGBRV LPP compared to the local part of GBRV.

System	KEDF	PP	$\Delta n/N_v$	Improvement (%)
	TF0.2vW	GBRV	0.291	71
	1F0.2VW	PGBRV0.2	0.074	75
	$_{ m TFvW}$	GBRV	0.291	56
	1 F V VV	PGBRV0.2	0.128	50
Dd	LKT	GBRV	0.268	58
$Pd_{13}$		PGBRV0.2	0.113	90
	revHC LMGP	GBRV	0.240	69
		PGBRV0.2	0.074	09
		GBRV	0.221	67
		PGBRV0.2	0.073	07

#### VI. CONCLUSIONS

In this study, we developed new sets of pseudopotentials for OF-DFT calculations targeting transition metal elements. Transition metals have historically been excluded from

TABLE VI. Relative density difference (against KS) for  $Ag_{20}$ . Other details as in Table V.

System	KEDF	PP	$\Delta n/N_v$	Improvement (%)
	TF0.2vW	GBRV	0.182	77
	1 F U. 2 V VV	PGBRV0.2	0.042	77
	$_{ m TFvW}$	GBRV	0.182	67
	1 F V VV	PGBRV0.2	0.059	07
Λœ	LKT	GBRV	0.164	77
$Ag_{20}$		PGBRV0.2	0.038	11
	revHC	GBRV	0.128	63
		PGBRV0.2	0.047	03
	LMGP	GBRV	0.107	22
	LIVIGE	PGBRV0.2	0.084	44

TABLE VII. Relative density difference (against KS) for  $Pt_{10}$ . Other details as in Table V.

System	KEDF	PP	$\Delta n/N$	Improvement (%)
	TF0.2vW	GBRV	0.290	70
	1 F U. 2 V VV	PGBRV0.2	0.061	79
	$\mathrm{TFvW}$	GBRV	0.290	56
	1 F V VV	PGBRV0.2	0.128	50
$Pt_{10}$	LKT	GBRV	0.277	62
1 010		PGBRV0.2	0.105	02
	revHC	GBRV	0.247	71
		PGBRV0.2	0.071	11
	LMGP	GBRV	0.241	72
	LIMGP	PGBRV0.2	0.067	12

OF-DFT applications due to the challenges of constructing suitable local pseudopotentials. The core idea of this work is to adapt existing KS-DFT pseudopotentials (specifically, PSL and GBRV) by imposing that OF-DFT calculations with approximate noninteracting kinetic energy functionals reproduce, as closely as possible, the electron density from KS-DFT cal-

culations of the element's most stable condensed phase. This approach effectively performs a KS-to-OF inversion near the ion cores. This opens the possibility to investigate large-scale metallic systems and nanostructures at the OF cost (linear scaling with low prefactor). However, we point out that simulations based on OF-DFT for transition metals should still be considered "highly experimental" and not yet ready for broad use.

Our convergence analysis shows that GBRV-based pseudopotentials generally outperform PSL pseudopotentials for most transition metals. Figure 6 summarizes our recommendations for each element: solid colors indicate successful pseudization, while hatched areas denote intermediate accuracy (see Figure caption for details).

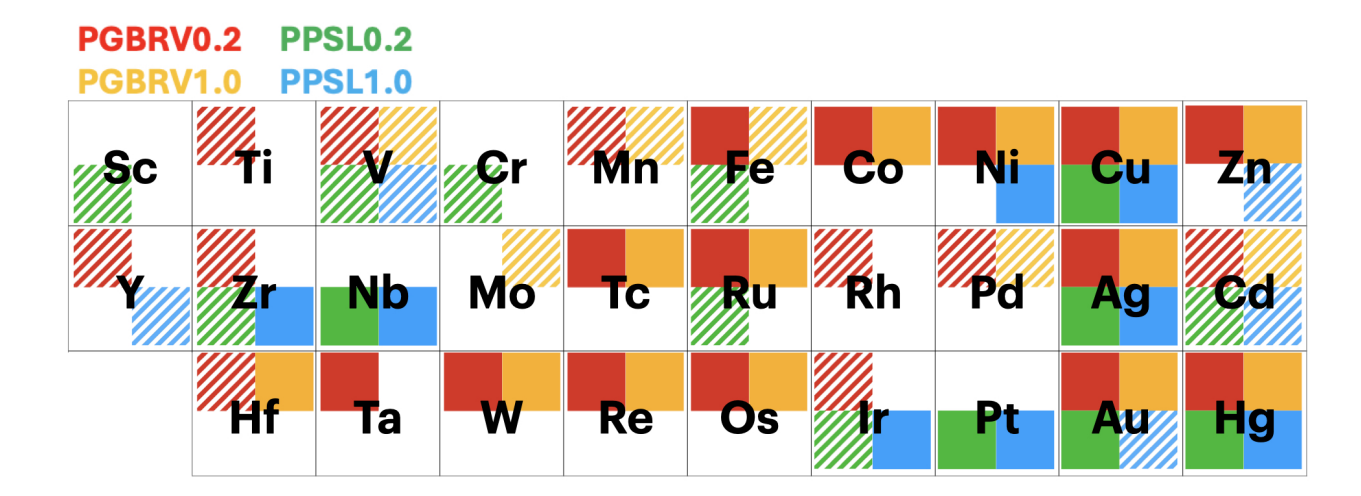


FIG. 6. Recommendations for using the proposed pseudopotentials. The color map illustrates the outcome of the pseudization procedure. Solid colors represent elements for which the pseudopotential yields accurate results; hatched areas indicate lower-quality pseudization; and uncolored elements correspond to pseudopotentials we consider inaccurate. These recommendations are based on three sets of data: the electron density in the bulk system, the electron density of the isolated atom, and equation of state parameters.

We conclude with a note of caution: there are still major challenges for applying OF-DFT methods to transition metals. While pseudopotentials are increasingly available (see, e.g., Refs. 17,18,26 and this work), the overall accuracy of existing physics-based OF-DFT methods is still insufficient for the widespread use of OF-DFT with these important elements.

#### VII. ACKNOWLEDGEMENTS

We thank ICTP and ASESMA (https://www.asesma.org) for promoting collaboration between the Pavanello group and EO, WFIE, SJO and AO. This work was supported by grants from the U.S. National Science Foundation under grant agreements CHE-2154760, OAC-2321103. The authors acknowledge the Office of Advanced Research Computing (OARC) at Rutgers, The State University of New Jersey for providing access to the Amarel cluster and associated research computing resources that have contributed to the results reported here. URL: https://it.rutgers.edu/oarc

#### REFERENCES

- <sup>1</sup>W. Kohn and L. J. Sham, "Self-consistent equations including exchange and correlation effects," Physical review **140**, A1133 (1965).
- <sup>2</sup>J. P. Perdew, K. Burke, and M. Ernzerhof, "Generalized gradient approximation made simple," Physical review letters **77**, 3865 (1996).
- <sup>3</sup>K.-H. Liou, C. Yang, and J. R. Chelikowsky, "Scalable implementation of polynomial filtering for density functional theory calculation in parsec," Computer Physics Communications **254**, 107330 (2020).
- <sup>4</sup>W. Dawson, A. Degomme, M. Stella, T. Nakajima, L. E. Ratcliff, and L. Genovese, "Density functional theory calculations of large systems: Interplay between fragments, observables, and computational complexity," Wiley Interdisciplinary Reviews: Computational Molecular Science 12, e1574 (2022).
- <sup>5</sup>T. Miyazaki, A. Nakata, and D. R. Bowler, "Large-scale first-principles calculation technique for nanoarchitectonics: Local orbital and linear-scaling dft methods with the conquest code," System-Materials Nanoarchitectonics, 303–317 (2022).
- <sup>6</sup>L. Xue, Q. Xu, C. Ma, W. Mi, Y. Wang, Y. Xie, and Y. Ma, "Accelerating ab initio real-space electronic structure calculations for low-dimensional materials using an atom-sphere grid truncation method," Physical Review B **110**, 155157 (2024).
- <sup>7</sup>W. Mi, K. Luo, S. Trickey, and M. Pavanello, "Orbital-free density functional theory: An attractive electronic structure method for large-scale first-principles simulations," Chem. Rev. **123**, 12039–12104 (2023).

- <sup>8</sup>W. C. Witt, B. G. Del Rio, J. M. Dieterich, and E. A. Carter, "Orbital-free density functional theory for materials research," Journal of Materials Research **33**, 777–795 (2018).
- <sup>9</sup>W. Mi and M. Pavanello, "Orbital-free density functional theory correctly models quantum dots when asymptotics, nonlocality, and nonhomogeneity are accounted for," Physical Review B **100**, 041105 (2019).
- <sup>10</sup>W. Mi and M. Pavanello, "Nonlocal subsystem density functional theory," The Journal of Physical Chemistry Letters **11**, 272–279 (2019).
- <sup>11</sup>C. Huang and E. A. Carter, "Nonlocal orbital-free kinetic energy density functional for semiconductors," Physical Review B **81**, 045206 (2010).
- <sup>12</sup>X. Shao, W. Mi, and M. Pavanello, "Revised huang-carter nonlocal kinetic energy functional for semiconductors and their surfaces," Physical Review B **104**, 045118 (2021).
- <sup>13</sup>B. Wang and M. Stott, "First-principles local pseudopotentials for group-iv elements," Physical Review B **68**, 195102 (2003).
- <sup>14</sup>S. Watson, B. Jesson, E. Carter, and P. Madden, "Ab initio pseudopotentials for orbital-free density functionals," Europhysics Letters 41, 37 (1998).
- <sup>15</sup>F. Legrain and S. Manzhos, "Highly accurate local pseudopotentials of li, na, and mg for orbital free density functional theory," Chemical Physics Letters **622**, 99–103 (2015).
- <sup>16</sup>J.-D. Chai and J. D. Weeks, "Orbital-free density functional theory: Kinetic potentials and ab initio local pseudopotentials," Physical Review B—Condensed Matter and Materials Physics 75, 205122 (2007).
- <sup>17</sup>Y.-C. Chi and C. Huang, "High-quality local pseudopotentials for metals," Journal of Chemical Theory and Computation **20**, 3231–3241 (2024).
- <sup>18</sup>W. Mi, S. Zhang, Y. Wang, Y. Ma, and M. Miao, "First-principle optimal local pseudopotentials construction via optimized effective potential method," The Journal of chemical physics **144** (2016).
- <sup>19</sup>Y. Ke, F. Libisch, J. Xia, L.-W. Wang, and E. A. Carter, "Angular-momentum-dependent orbital-free density functional theory," Physical review letters 111, 066402 (2013).
- <sup>20</sup>K. F. Garrity, J. W. Bennett, K. M. Rabe, and D. Vanderbilt, "Pseudopotentials for high-throughput dft calculations," Computational Materials Science **81**, 446–452 (2014).
- <sup>21</sup>D. Hamann, M. Schlüter, and C. Chiang, "Norm-conserving pseudopotentials," Physical review letters **43**, 1494 (1979).

- <sup>22</sup>C. Huang and E. A. Carter, "Transferable local pseudopotentials for magnesium, aluminum and silicon," Physical Chemistry Chemical Physics **10**, 7109–7120 (2008).
- <sup>23</sup>B. Zhou, Y. A. Wang, and E. A. Carter, "Transferable local pseudopotentials derived via inversion of the kohn-sham equations in a bulk environment," Physical Review B **69**, 125109 (2004).
- <sup>24</sup>B. G. Del Rio, J. M. Dieterich, and E. A. Carter, "Globally-optimized local pseudopotentials for (orbital-free) density functional theory simulations of liquids and solids," Journal of Chemical Theory and Computation 13, 3684–3695 (2017).
- <sup>25</sup>T. Starkloff and J. Joannopoulos, "Local pseudopotential theory for transition metals," Physical Review B **16**, 5212 (1977).
- <sup>26</sup>Q. Xu, C. Ma, W. Mi, Y. Wang, and Y. Ma, "Nonlocal pseudopotential energy density functional for orbital-free density functional theory," Nature Communications 13, 1385 (2022).
- <sup>27</sup>D. Chakraborty, R. Cuevas-Saavedra, and P. W. Ayers, "Two-point weighted density approximations for the kinetic energy density functional," Theoretical Chemistry Accounts **136**, 1–12 (2017).
- <sup>28</sup>T. L. Gilbert, "Hohenberg-kohn theorem for nonlocal external potentials," Physical Review B 12, 2111 (1975).
- <sup>29</sup>L. Kleinman and D. Bylander, "Efficacious form for model pseudopotentials," Physical review letters **48**, 1425 (1982).
- <sup>30</sup>A. Görling, "Orbital-and state-dependent functionals in density-functional theory," The Journal of chemical physics 123 (2005).
- <sup>31</sup>W. Yang and Q. Wu, "Direct method for optimized effective potentials in density-functional theory," Physical Review Letters **89**, 143002 (2002).
- <sup>32</sup>C. R. Jacob, "Unambiguous optimization of effective potentials in finite basis sets," The Journal of chemical physics 135 (2011).
- <sup>33</sup>D. S. Jensen and A. Wasserman, "Numerical methods for the inverse problem of density functional theory," International Journal of Quantum Chemistry **118**, e25425 (2018).
- <sup>34</sup>Z. A. Moldabekov, X. Shao, M. Pavanello, J. Vorberger, and T. Dornheim, "Nonlocal vs local pseudopotentials affect kinetic energy kernels in orbital-free dft," Electronic Structure 7, 015006 (2025).

- <sup>35</sup>X. Shao, O. Andreussi, D. Ceresoli, M. Truscott, A. Baczewski, Q. Campbell, and M. Pavanello, "QEpy: Quantum ESPRESSO in Python," https://gitlab.com/shaoxc/qepy.
- <sup>36</sup>P. Giannozzi, S. Baroni, N. Bonini, M. Calandra, R. Car, C. Cavazzoni, D. Ceresoli, G. L. Chiarotti, M. Cococcioni, I. Dabo, et al., "Quantum espresso: a modular and open-source software project for quantum simulations of materials," Journal of physics: Condensed matter 21, 395502 (2009).
- <sup>37</sup>H. J. Monkhorst and J. D. Pack, "Special points for brillouin-zone integrations," Phys. Rev. B 13, 5188–5192 (1976).
- <sup>38</sup>K. F. Garrity, J. W. Bennett, K. M. Rabe, and D. Vanderbilt, "Pseudopotentials for high-throughput dft calculations," Computational Materials Science **81**, 446–452 (2014).
- <sup>39</sup>A. Dal Corso, "Pseudopotentials periodic table: From h to pu," Computational Materials Science **95**, 337–350 (2014).
- <sup>40</sup>X. Shao, K. Jiang, W. Mi, A. Genova, and M. Pavanello, "Dftpy: An efficient and object-oriented platform for orbital-free dft simulations," WIREs: Comp. Mol. Sci. **11**, e1482 (2021).
- <sup>41</sup>J. P. Perdew and A. Zunger, "Self-interaction correction to density-functional approximations for many-electron systems," Physical review B **23**, 5048 (1981).
- <sup>42</sup>C. L. Fu and K. M. Ho, "First-principles calculation of the equilibrium ground-state properties of transition metals: Applications to nb and mo," Phys. Rev. B **28**, 5480–5486 (1983).
- <sup>43</sup>Q. Xu, Y. Wang, and Y. Ma, "Nonlocal kinetic energy density functional via line integrals and its application to orbital-free density functional theory," Physical Review B **100**, 205132 (2019).
- <sup>44</sup>X. Gonze, "First-principles responses of solids to atomic displacements and homogeneous electric fields: Implementation of a conjugate-gradient algorithm," Physical Review B **55**, 10337 (1997).
- <sup>45</sup>S. Baroni, S. De Gironcoli, A. Dal Corso, and P. Giannozzi, "Phonons and related crystal properties from density-functional perturbation theory," Reviews of modern Physics **73**, 515 (2001).
- <sup>46</sup>X. Shao, W. Mi, and M. Pavanello, "Efficient dft solver for nanoscale simulations and beyond," The Journal of Physical Chemistry Letters **12**, 4134–4139 (2021).

- <sup>47</sup>L. Fiedler, Z. A. Moldabekov, X. Shao, K. Jiang, T. Dornheim, M. Pavanello, and A. Cangi, "Accelerating equilibration in first-principles molecular dynamics with orbital-free density functional theory," Physical Review Research 4, 043033 (2022).
- <sup>48</sup>L. A. Constantin, E. Fabiano, S. Laricchia, and F. Della Sala, "Semiclassical neutral atom as a reference system in density functional theory," Physical review letters **106**, 186406 (2011).
- <sup>49</sup>V. Rios-Vargas, X. Shao, S. Trickey, and M. Pavanello, "Effective wang-teter kernels for improved orbital-free density functional theory simulations," Physical Review B **110**, 085129 (2024).
- <sup>50</sup>W. C. Witt, B. W. Shires, C. W. Tan, W. J. Jankowski, and C. J. Pickard, "Random structure searching with orbital-free density functional theory," The Journal of Physical Chemistry A 125, 1650–1660 (2021).
- <sup>51</sup>S. Laricchia, E. Fabiano, L. Constantin, and F. Della Sala, "Generalized gradient approximations of the noninteracting kinetic energy from the semiclassical atom theory: Rationalization of the accuracy of the frozen density embedding theory for nonbonded interactions," Journal of chemical theory and computation 7, 2439–2451 (2011).